

# Towards a Shock Tube Method for the Dynamic Calibration of Pressure Sensors

Stephen Downes, Andy Knott\*, Ian Robinson

National Physical Laboratory, Hampton Road, Teddington, United Kingdom TW11 0LW

\* Andy Knott, "Force Metrology", National Physical Laboratory, UK, e-mail: andy.knott@npl.co.uk

Updated version of the original article in **Philosophical Transactions A of the Royal Society**, DOI: 10.1098/rsta.2013.0299

## Abstract

In theory shock tubes provide a pressure change with a very fast rise time and calculable amplitude. This pressure step could provide the basis for the calibration of pressure transducers used in highly dynamic applications. However, conventional metal shock tubes can be expensive, unwieldy, and difficult to modify. We describe the development of a 1.4 MPa (maximum pressure) shock tube made from PVC-U pressure tubing which provides a low-cost, light, and easily modifiable basis for establishing a method for determining the dynamic characteristics of pressure sensors.

## 1 Introduction

Many pressure measurements are made dynamically, as there is the need to measure pressures which are rapidly changing. It is necessary to show that the sensor's output provides an accurate representation of the pressure throughout the measurements [1–3]. At present, many sensors used in such applications are only calibrated using static methods due to the difficulty of generating known pressure changes of the required rate and amplitude. An example can be found in combustion engines where the in-cylinder pressure varies periodically from 0.1 MPa to 10 MPa, at frequencies of up to 30 kHz [4–6]. The pressures are measured using electro-mechanical sensors, which are calibrated statically, and it is not known if their dynamic characteristics cause their statically-determined sensitivity to change as the frequency increases. This can lead to errors in the measured pressures and may also cause problems if a sensor has to be replaced. If sensors are calibrated both statically and dynamically, the reliability and uncertainty of the measurements will be improved.

Dynamic calibration requires a source with known characteristics in both amplitude and frequency. A shock wave generated in a shock tube has a rise time of the order of 1 ns and the amplitude of the pressure step generated upon reflection of the wave from the end face of the

tube can be calculated. This makes it an ideal candidate for a pressure calibration standard if it can be verified that the magnitude of the pressure step can be determined accurately from ideal gas theory using readily-measured parameters such as shock wave velocity and static temperatures and pressures. We have investigated the application of a novel shock tube, made from plastic tubing, to the determination of the frequency response of pressure sensors and have made significant progress towards extending SI pressure measurements to the dynamic regime.

As the aim of this investigation is to provide a means of calibrating the dynamic response of pressure sensors, the theory cannot be validated simply by comparing the measured and the calculated pressures. It is assumed that the pressure indicated by the sensors is independent of the gas species and, at present, it is also assumed that the sensors are linear and that the uncertainties associated with non-ideal behaviour of the gases are significantly lower than those associated with the experimental measurements. By comparing the theoretical and measured values of the pressure steps for different pressures and gas species it should be possible both to assess the quality of the measurement system and determine the dynamic calibration of the sensor. However this task is complicated by the non-ideal behaviour of both the shock tube and the sensor, both of which are investigated here.

## 2 Shock Tube Theory

A simple shock tube consists of two straight tubes of the same circular cross-section that are separated by a diaphragm. One tube contains a low pressure "driven" gas and the other is filled with a "driver" gas. Gas is added to the driver side until the diaphragm ruptures allowing the driver gas to generate a series of compression waves within the driven gas which coalesce to form a shock wave that propagates into the remaining undisturbed driven gas. The release of pressure at the diaphragm causes an expansion wave to propa-

gate back into the driver section. Simultaneously, a contact surface between the driver and driven gases, which moves more slowly than the shock wave, propagates along the tube behind the shock front. The length of the driven tube section and the relative velocity between the shock wave and contact surface ultimately determine the time over which useful measurements can be made.

The pressures, temperatures, and densities generated within a uniform diameter, low-pressure shock tube can be derived from ideal gas theory. The shock front has a thickness of a few hundred nanometres [7]; thus, to an observer at rest, the pressure across a shock wave moving at  $500 \text{ m}\cdot\text{s}^{-1}$  rises from its initial value to its relatively constant post-shock value in a time period of the order of a nanosecond. The pressure remains constant for a few milliseconds after the shock wave has passed depending on the tube dimensions, sensor location, gas species used in the driver and driven sections, and the starting pressures and temperatures. The pressure change can therefore be considered as a step generating all frequencies above a low frequency limit, which is proportional to the reciprocal of the time that the pressure remains constant.

Figure 1 shows the stages of operation of a shock tube. Figure 1a shows the condition of the tube at the point that the diaphragm bursts. The driver section is at a uniform pressure  $p_4$  and temperature  $T_4$  and the driven section is at a uniform pressure  $p_1$  and temperature  $T_1$ . In figure 1b the diaphragm has burst and the shock front is

propagating into the driven gas with a constant pressure  $p_2$  behind the shock. The contact surface between the driven and driver gases is propagating in the same direction as the shock front but at a lower speed. In figure 1c the rarefaction wave has reflected from the end of the driver section and the reflected rarefaction wave is propagating towards the other end of the tube. In figure 1d the shock wave has reflected from the end of the tube and the pressure in the end section has risen to  $p_5$  with an associated temperature  $T_5$ . The reflected shock wave propagates back into the part of the tube at pressure  $p_2$  until it meets the contact surface where it is partially reflected and partially transmitted. At the time of arrival of the shock wave a sensor in the centre of the end wall of the tube would see a pressure step of amplitude  $(p_5 - p_1)$  and the measured pressure would remain stable at  $p_5$  until the arrival of the shock wave reflected from the contact surface.

The magnitude of this step can be determined from ideal gas theory; the analysis can be found in [8–10], and is reproduced below. The pressure  $p_2$  is calculated from a knowledge of  $p_1$ ,  $\gamma_1$  (the ratio of the specific heat at constant pressure to that at constant volume for the driven gas), and the Mach number  $M_s$  of the advancing shock wave:

$$p_2 = p_1 \left( 1 + \frac{2\gamma_1}{\gamma_1 + 1} (M_s^2 - 1) \right) .$$

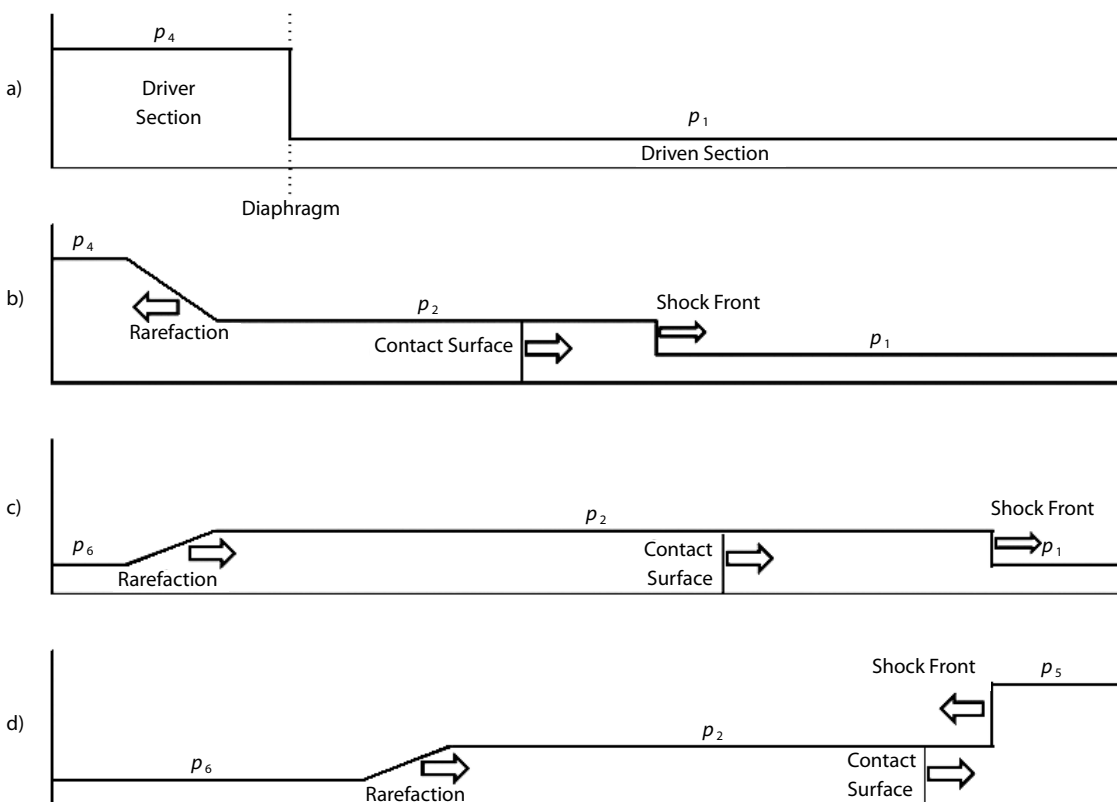


Figure 1: Shock tube operation.

The Mach number of the shock is the ratio of the speed of the shock wave to the speed of sound  $a_1$  in the undisturbed driven gas. The speed of the shock wave is calculated from measurements of the times that the shock wave passes two pressure sensors mounted a known distance apart in the wall of the tube. The speed of sound

$$a_1 = \sqrt{\frac{\gamma_1 R T_1}{m_1}},$$

where  $T_1$  is the measured initial temperature (in K) of the driven gas,  $m_1$  is its molecular weight and  $R$  is the gas constant.

The pressure  $p_5$  existing after reflection of the shock from the end wall can be calculated from  $p_1$ ,  $p_2$ , and  $\alpha_1 = (\gamma_1 + 1)/(\gamma_1 - 1)$ :

$$p_5 = p_2 \left( \frac{(\alpha_1 + 2) \frac{p_2}{p_1} - 1}{\frac{p_2}{p_1} + \alpha_1} \right).$$

For a specific driven gas at a known starting pressure, the magnitude of the pressure step ( $p_5 - p_1$ ) is simply a function of the shock wave Mach number; for air ( $\gamma_1 \approx 1.4$ ) starting at atmospheric pressure ( $p_1 \approx 0.1$  MPa) and room temperature, this function is shown in figure 2.

$M_s$  increases with the pressure ratio across the diaphragm; it can be increased further by increasing the speed of sound in the driver gas, either by heating it or by using a lighter gas, such as helium or hydrogen.

The relationship between the driver pressure  $p_4$ , the driven pressure  $p_1$  and the Mach number  $M_s$  is given by:

$$\frac{p_4}{p_1} = \frac{1}{\alpha_1} \left( \frac{2\gamma_1 M_s^2}{\gamma_1 - 1} - 1 \right) \left( 1 - \frac{\left( \frac{1}{\alpha_4} \right) \left( \frac{a_1}{a_4} \right) (M_s^2 - 1)}{M_s} \right)^{\frac{-2\gamma_4}{\gamma_4 - 1}},$$

where  $\gamma_4$  is the ratio of specific heats for the driver gas,  $\alpha_4 = (\gamma_4 + 1)/(\gamma_4 - 1)$  and  $a_4$  is the speed of sound in the undisturbed driver gas. Figure 3 shows the pressure step ( $p_5 - p_1$ ) for air, helium, and argon as a function of the pressure  $p_1$  in the driven section for a constant pressure  $p_4 = 1.4$  MPa of nitrogen in the driver section.

The temperature  $T_5$  of the gas after the reflection of the shock wave can be calculated from the following equations:

$$\frac{T_2}{T_1} = \frac{p_2}{p_1} \left( \frac{\alpha_1 + \frac{p_2}{p_1}}{1 + \alpha_1 \frac{p_2}{p_1}} \right)$$

and

$$\frac{T_5}{T_2} = \frac{p_5}{p_2} \left( \frac{\alpha_1 + \frac{p_5}{p_2}}{1 + \alpha_1 \frac{p_5}{p_2}} \right).$$

The assumption that the gases behave ideally will not hold if the molecular energies produced by the generation and reflection of the shock wave are not significantly lower than the dissociation and ionization energies of the gases used (typically greater than 5 eV). Figure 4 shows the temperature of the driven gas after the reflection of the shock wave from the end of the tube. The results are calculated for a pressure of 1.4 MPa in the driver section. The thermal energy associated with this

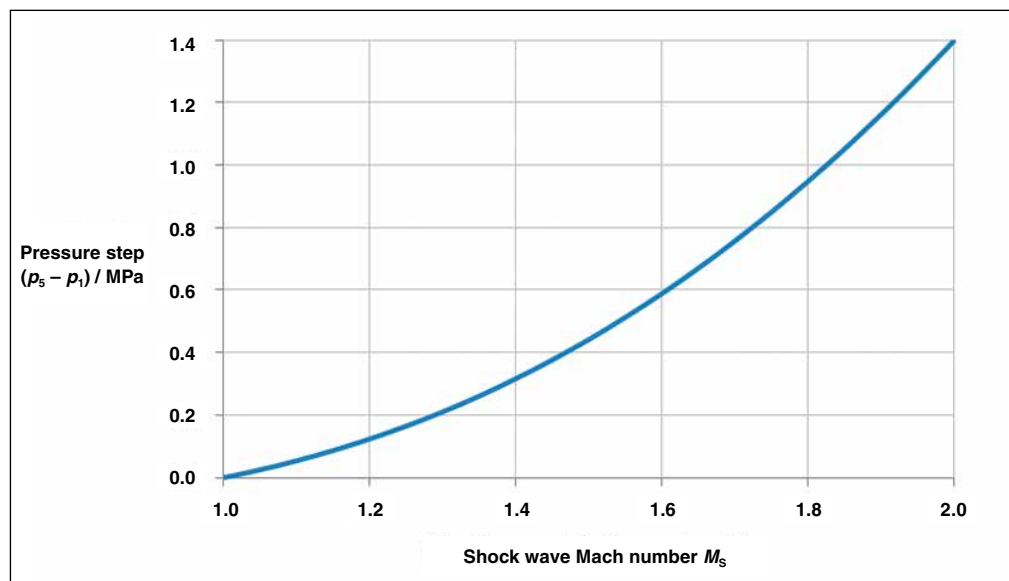


Figure 2: Pressure step versus shock wave Mach number.

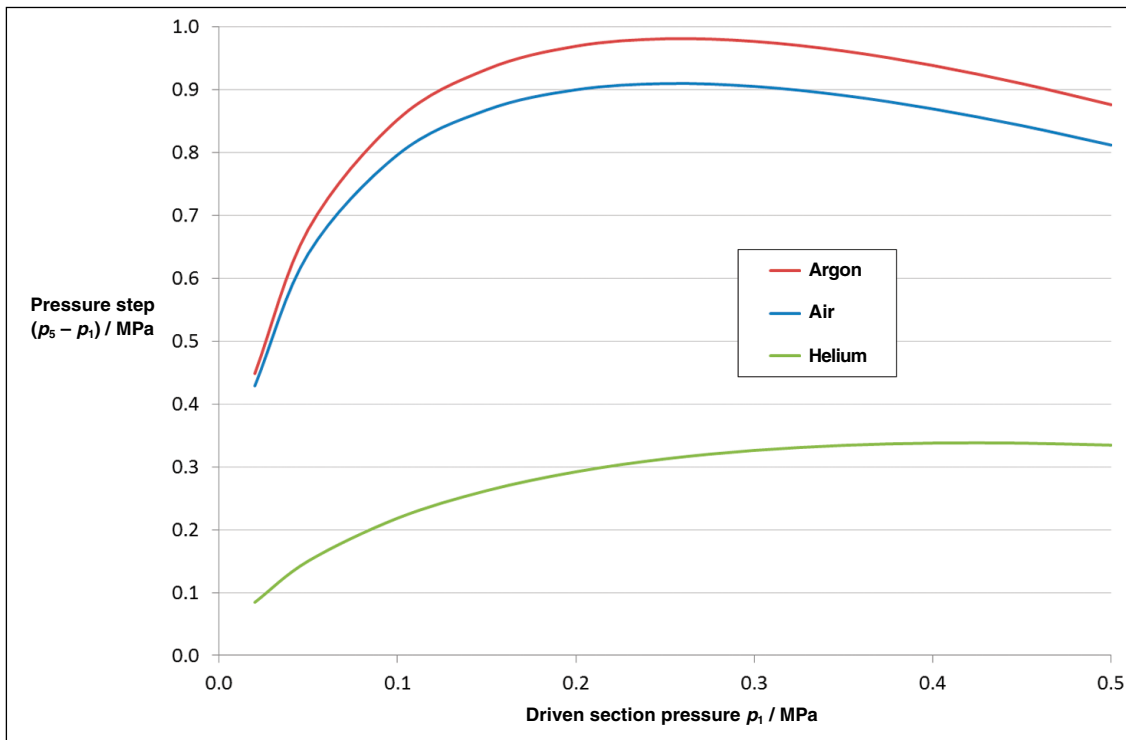


Figure 3: Generated pressure step versus initial driven pressure.

temperature is  $kT/e$  eV where  $k$  is the Boltzmann constant and  $e$  is the elementary charge. Argon at 0.02 MPa reaches a temperature of 1300 K with an equivalent energy of 0.11 eV. Typical operation of the tube with air at 0.1 MPa reaches a temperature of 600 K with an equivalent energy of 0.05 eV. These energies are orders of magnitude below the dissociation and ionization energies of the gases used, and the temperatures reached in this shock tube are therefore insufficient to cause significant deviations from ideal gas behaviour.

### 3 Construction of the Shock Tube

Conventional shock tubes are made from metal tubing and are costly, heavy and relatively difficult to modify. The shock tube described below (and shown in figure 5) differs from conventional designs in that it is made from plastic tubing. This makes it cheap to manufacture, it is light enough so that the longest (6 m) section can be readily manoeuvred by one person, and it can be constructed and modified using readily available tools.

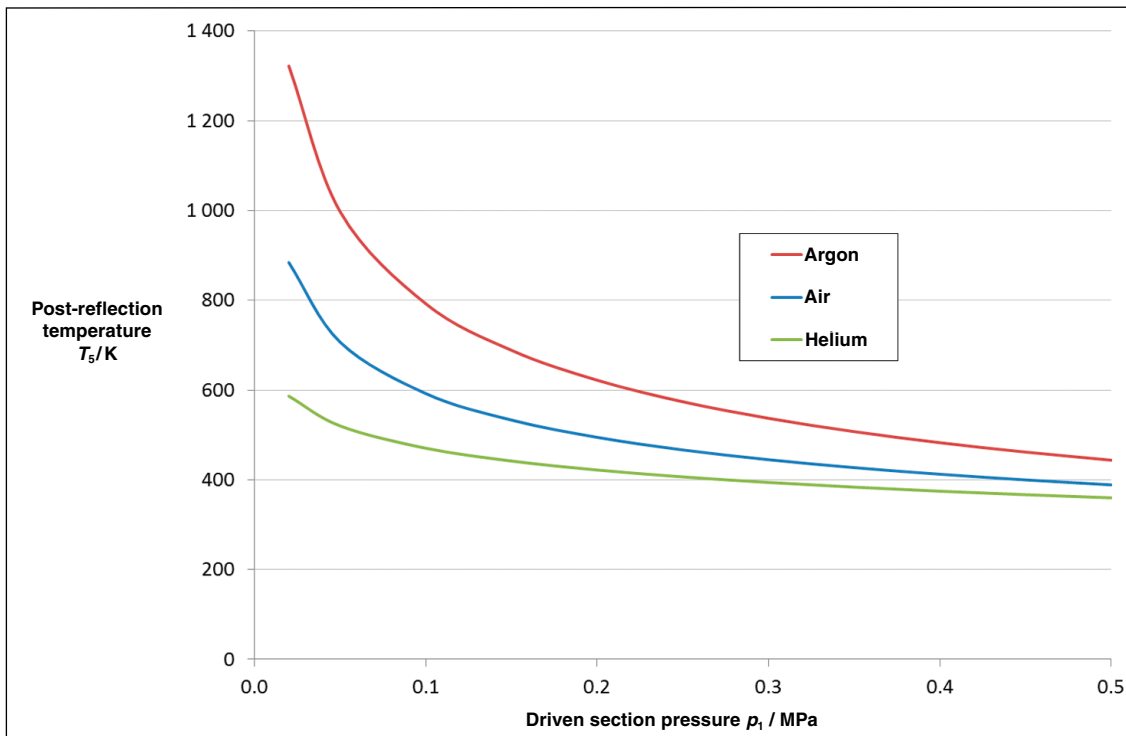


Figure 4: Post-reflection temperature versus initial driven section pressure.

The shock tube is manufactured from 76 mm i/d PVC-U tube with a 6.5 mm thickness wall which the manufacturers claim is suitable for use with gases with a maximum static working pressure of 1.5 MPa. The completed tube sections were limited to a working pressure of 1.4 MPa and were tested at a pressure approximately 50 % higher than this for a few minutes to ensure that they were safe for routine use at the working pressure. The pipe is cut to the required length and commercial plastic pipe flange adaptors, turned down to an outer diameter of just less than 123 mm, are glued to each end of the pipe and equipped with steel flanges. The flanges allow the pipe sections to be connected using four M16 steel bolts. Steel rings 6 mm thick with o-ring slots on both faces (shown in figure 6) are used to provide reliable seals between the faces of the flange adaptors and other parts of the shock tube. Driven sections of 2 m, 4 m, and 6 m in length have been constructed along with a 0.7 m driver section. The length of the driver section was chosen to limit the pressure-volume (PV) product to 4.5 kJ for a gas pressure of 1.4 MPa which is less than the 5 kJ statutory limit for this type of equipment. Most of the remaining parts – the pressurization flanges, the buffer section, and the sensor holder – were turned from an acetal rod.

#### 4 Generating the Shock Wave

The rupture of a metal diaphragm caused by gas pressure provides a simple method for producing a shock wave. However, for a given thickness of diaphragm, the burst pressure will be fairly consistent and, unless a large range of thicknesses of material is available, this will limit the shock pressures that can be investigated. To provide a selectable

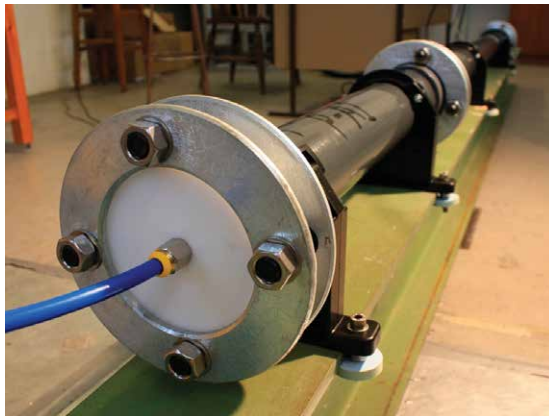


Figure 5:  
NPL 1.4 MPa  
shock tube.



Figure 6:  
A steel ring with  
o-rings mounted  
in each face.

pressure in the driver gas, an alternative technique uses two diaphragms separated by a small distance (25 mm–30 mm). This creates a third chamber in the shock tube: the “buffer”. If, during pressurization, the pressure in the buffer is maintained at half the pressure in the driver section, it is possible to raise the pressure in the driver section to any pressure between one and two times the bursting pressure of the diaphragms. If the gas in the buffer is then vented, both diaphragms will burst in a rapid sequence producing the required shock wave driven by the chosen pressure in the driver section.

The tube described can be used in either single or double diaphragm mode. In single diaphragm mode, the diaphragm is clamped between the plastic flanges terminating the tubes of the driver and driven sections. Intermediate steel ring and o-ring components (figure 6) ensure a good seal and prevent distortions of the diaphragm material which can produce leaks. The most effective diaphragm material for the generated driver pressures has been brass shim of either 0.1 mm or 0.05 mm thickness. The shim is supplied in rolls and is cut to fit the steel rings. The 0.1 mm sheet repeatedly bursts at a gauge pressure (i.e. a pressure above atmospheric) of approximately 1.35 MPa while the 0.05 mm sheet bursts at about 0.84 MPa.

In the double diaphragm arrangement, the two diaphragms are situated either side of a small buffer section which consists of a 29 mm thick acetal ring which can be pressurized independently of the driver and is pressurized as described above. To initiate diaphragm rupture, a local solenoid valve is operated to vent the buffer to atmosphere. Whilst this method provides the advantage of a selectable burst pressure it has the disadvantage of using twice as much diaphragm material for each operation of the tube and is more complex to set up as both diaphragms and the buffer ring have to be carefully positioned before the tube sections are clamped together.

The single diaphragm method has been used for most of the investigations in this study as it is simple and reliable, and the two burst pressures, which can be obtained with commercially available shim thicknesses, are usually sufficient.

#### 5 Control System

The driver section is pressurized using bottled gas, initially nitrogen but helium and argon can also be used. The control system for the tube is fully automated using computer-controlled solenoid valves, temperature and pressure sensors.

The system is controlled by a program written in Python on a laptop computer running Linux. An Agilent 34970A data acquisition/switch unit, connected to the computer via a serial link, is used to interface to the shock tube. A digital interface

on the switch unit connects to a custom-built driver for the eight mains-operated solenoid valves needed to control the tube; the multiplexed voltmeter in the switch unit is used to measure both the voltages from the pressure transducers and the resistance of the platinum resistance thermometers.

Two gas manifolds are used: a high pressure manifold supplying the driver and buffer sections of the tube and a low pressure manifold supplying the driven section. A pressure transducer on the high pressure manifold enables the computer to determine if there is sufficient pressure in the manifold to operate the tube.

Three gas handling channels are provided which control the driver section, the buffer section, and the driven section. Each channel has a solenoid valve which vents the associated section to atmosphere and a pressure relief valve to ensure that the parts of the tube cannot be pressurized beyond their maximum working pressure. Each channel also has a solenoid valve and flow control valve which allow each section to be filled from its associated manifold at a controllable rate. The rate is set to allow time for pressure measurements to be made and acted upon by the computer to ensure accurate control of the pressure in each section of the tube. The pressure transducer for the driver section is mounted close to the pressurization port on the end flange of the driver to minimize measurement errors caused by flow-induced pressure drops in the supply tubing. In addition, to increase the speed of venting of the buffer section, the solenoid valve which vents it is mounted directly next to it. The driven section is provided with two extra solenoid valves. One isolates the driven section from the gas handling system to avoid the chance of damage to the pressure transducer caused by

the rapid, possibly over-range, pressure changes which accompany the firing of the tube. The other connects a vacuum pump to the driven section to allow gas to be removed so that the section can be either used at different pressures or filled with pure gas for measurements involving gases other than air.

The temperature of the gas in the driven section is inferred from measurements of the resistance of general purpose Pt100 platinum resistance thermometers which are placed in good contact with the walls of the tube. The gas is left for a few minutes to come to thermal equilibrium with the walls before a firing and the temperatures near the two ends of the tube are measured; the thermometers are then removed from their wells to avoid their being destroyed by the accelerations of the tube which accompany a firing.

## 6 Shock Pressure Measurements

Two pressure sensors in the side wall of the driven section are used to derive the velocity, and thereby the Mach number, of the shock wave by measuring the time delay between shock detections, as demonstrated by figure 7 (derived from a different shock tube set-up). The sensors are at right angles to the shock front and so, although the shock wave has a rise time of the order of 1 ns, the rise time of the pressure recorded by the sensor is proportional to the diameter of the sensor diaphragm divided by the shock velocity. For the conditions in this shock tube, this time is of the order of 10  $\mu$ s. The velocity can then be calculated from the known 400 mm separation between the sensors and the measured time interval between the two detections, with an uncertainty of approximately 1%. This uncertainty is largely derived from our

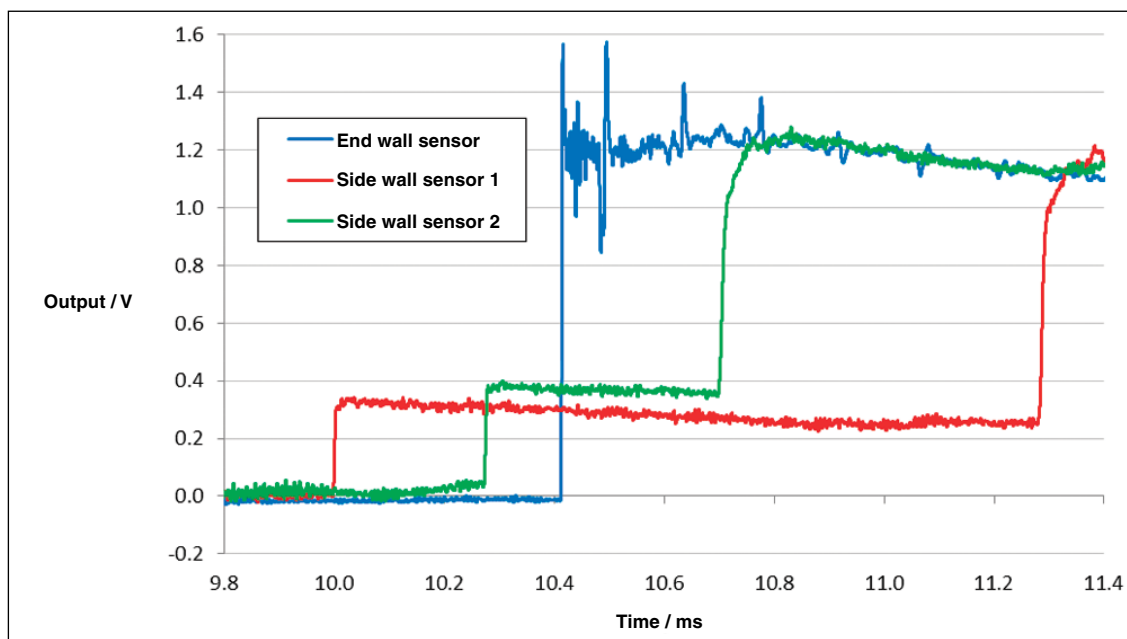


Figure 7: Estimation of the shock wave velocity. As the shock wave propagates down the driven section it first passes sensor 1 and then sensor 2 before reflecting from the end wall and travelling back past these two sensors.

present knowledge of the equality of the rise time of the sensors and charge amplifiers in response to the shock wave passing over the sensor diaphragm. In future, with further investigations, this uncertainty can be reduced considerably. The sensor having its dynamic response characterized is mounted centrally on the end wall of the driven section with its surface flush with the wall. Four identical piezoelectric sensors (Kistler model 603B) were used in this study; they have a 20 MPa input range with a natural frequency specified to be approximately 300 kHz. The output of each piezoelectric sensor was connected to a charge amplifier (Kistler 5015A) having a 200 kHz low pass filter on its voltage output. The outputs of the charge amplifiers are sampled synchronously using a flexible resolution digitizer (National Instruments PXI5922) having a resolution greater than 20 bits and a sampling rate of 2 MHz. Data is taken for a time of 200 ms with 10 ms of data acquired before the trigger event. The sampler is triggered on the rising edge of the output of the pressure transducer in the end wall of the shock tube.

## 7 Validating the Applicability of the Theory to the Operation of the Shock Tube

Ideal gas theory predicts that a perfect step, lasting several milliseconds, should be recorded by the data acquisition system when the shock wave is reflected from the end wall of the tube. However, in practice, many effects will prevent such an ideal event being recorded. For example, it has long been established that the pressure and temperature do not remain perfectly stable behind the reflected shock front [11–12]; but these and other effects must be investigated both directly and indirectly to eliminate/reduce their impact and to provide an estimate of the accuracy with which the pressure transducer can be calibrated by application of the ideal gas theory. The effects investigated include the following.

The effects of the diaphragm and tube length: the diaphragm does not open instantaneously and this could have an effect on the shock wave shape. The opening times of diaphragms vary considerably even within a single batch of diaphragm material, and the effect is likely to diminish with distance from the diaphragm. It is necessary to investigate the effect of differing diaphragms and the length of the tube on the shape of the pressure step.

The effects of secondary shock waves: these can be generated by the interaction of the main shock wave with imperfections in the tube; either on the inner surface of the tube or in the junction between the tube and the end wall. These secondary shock waves pass over the sensor following the

reflection of the main shock and generate transient signals in the sensor output. The effect of these must be eliminated from the measurement.

The effects of accelerations: the firing of the tube and the reflection of shock and rarefaction waves cause accelerations of the tube wall and the sensor mount. Modern pressure sensors used in dynamic applications can be designed to be relatively insensitive to accelerations but investigations need to be made to characterize the effects of acceleration on the pressure measurements.

The effects of varying the gas species and initial pressure: changing the species and pressure of the driven gas constitutes a powerful test for the agreement between theory and practice. The theory used to derive figure 2 predicts the pressure step given a measurement of the velocity of the shock wave and the initial static pressure and temperature in the driven section. The results for differing gases/pressures can be compared by assuming that a stable, linear pressure sensor is used to measure the pressure step. The quality of the agreement between results for monatomic and diatomic gases of differing molecular weights provides a good test of both the theory and the practice in the particular environment of this shock tube and leads to a way of calibrating the pressure sensor.

## 8 Test Results

### 8.1 Diaphragm material

The theory of the shock tube assumes that the diaphragm is removed instantaneously at the time the tube is fired. This does not happen in practice and the diaphragm opens over a period of a few hundred microseconds. However as the shock wave moves ahead of the contact surface, created by the opening of the diaphragm, it will encounter undisturbed gas and after a short time its shape should be largely independent of how it was formed as long as the diaphragm does open fully in a relatively short time. Tests were carried out to assess the influence of different diaphragm materials and, by implication, differing opening characteristics, on the shape of the generated dynamic pressure signal. Diaphragms of aluminium, brass, and copper, of various thicknesses, were burst and the resulting pressure transducer waveforms are shown in figure 8 (to aid comparison, these have been normalized to a value of 1.0 corresponding to the initial peak output after arrival of the shock front).

These results are some of the first to be taken with the plastic shock tube and the sensor was mounted at the end of the tube close to the plane of the flange adaptor. In this position there are many features in the wall of the shock tube which can produce reflected shock waves moving across the tube and this is likely to be the cause of the

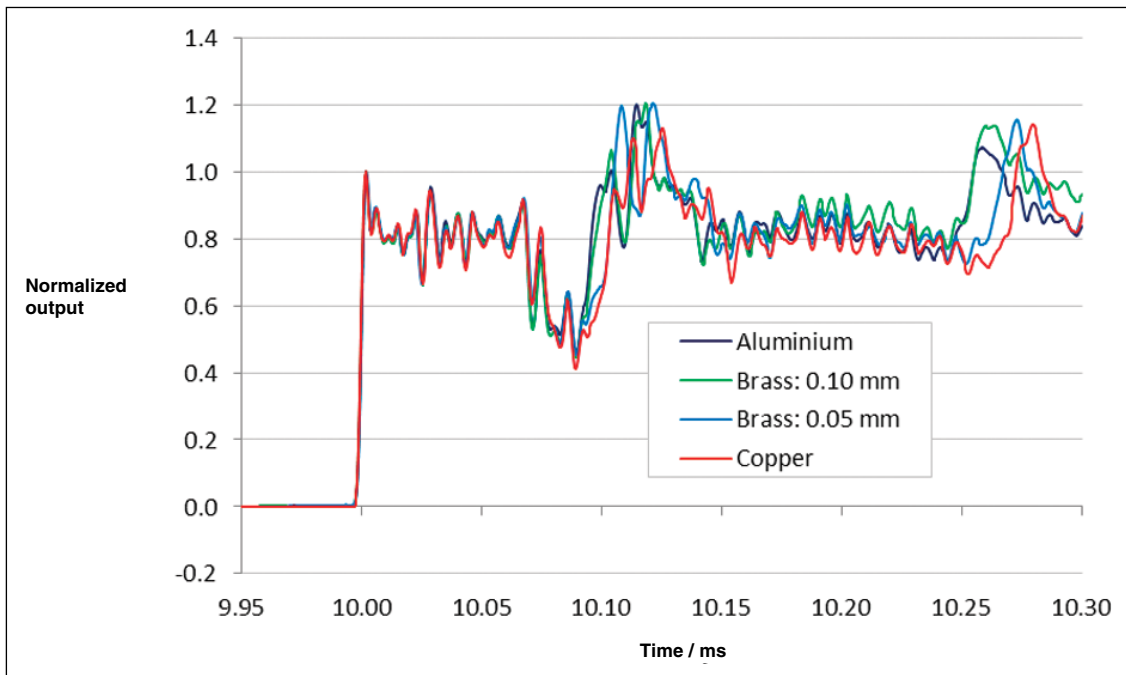


Figure 8: Comparison of diaphragm materials used in a single diaphragm arrangement. Burst pressures of approximately 1.3 MPa were obtained with the aluminium and brass (0.1 mm) diaphragms and approximately 0.8 MPa for copper and brass (0.05 mm).

feature seen in the period from 10.07 ms to 10.14 ms. The response of the transducer to the shock front in the first 0.06 ms is almost identical in all four cases suggesting that possible variations in the shock front due to differing diaphragm materials are insignificant when compared with other features seen in the output (possibly due to ringing in the dynamic response of the transducer).

## 8.2 Modifications to the sensor mount

In an attempt to reduce the magnitude of the pressure signal feature seen after 10.07 ms, the 70 mm diameter, 25 mm deep steel sensor holder was incorporated within a machined 80 mm long acetal rod which was bolted to an acetal flange. Figure 9 shows the rod and flange with a brass sensor holder. The rod diameter was adjusted to be a close fit within the tube. This moved the point at which the shock wave was reflected into the uniform section of the tube, providing fewer features to generate strong secondary shocks. The acetal rod was machined to leave an approximately 0.5 mm high annular lip around the steel sensor holder which could be removed later to determine the importance of such small features in generating secondary shock waves.

## 8.3 Driven section length / Burst pressure / Diaphragm configuration

With the location of the sensor mount altered, further tests were carried out with the two different thickness brass diaphragms, with different driven lengths, and with both single and double diaphragm



Figure 9: Acetal sensor mount showing annular lip that was machined flush with the insert (a brass insert is shown here).

arrangements. The results are shown in figure 10.

It is apparent that the periodic content of the output trace seems relatively unaffected by the various different experimental variations, particularly in the initial 0.06 ms period after arrival of the shock front, suggesting that these variations are of secondary importance. It can also be seen that the feature from 10.07 ms has changed significantly, and repeatably for the four different loading cases, from the previous experimental conditions, and that the pressure continues to vary significantly within the succeeding 0.05 ms period.

## 8.4 Further modifications to the transducer mount

The annular lip, left on the acetal rod (figure 9), was machined and then polished flush with the steel sensor holder. Figure 11 compares the results obtained in the two subsequent tests with those from the previous runs using the 0.1 mm brass diaphragm material and a 4 m driven section.

It is clear that this modification has significantly

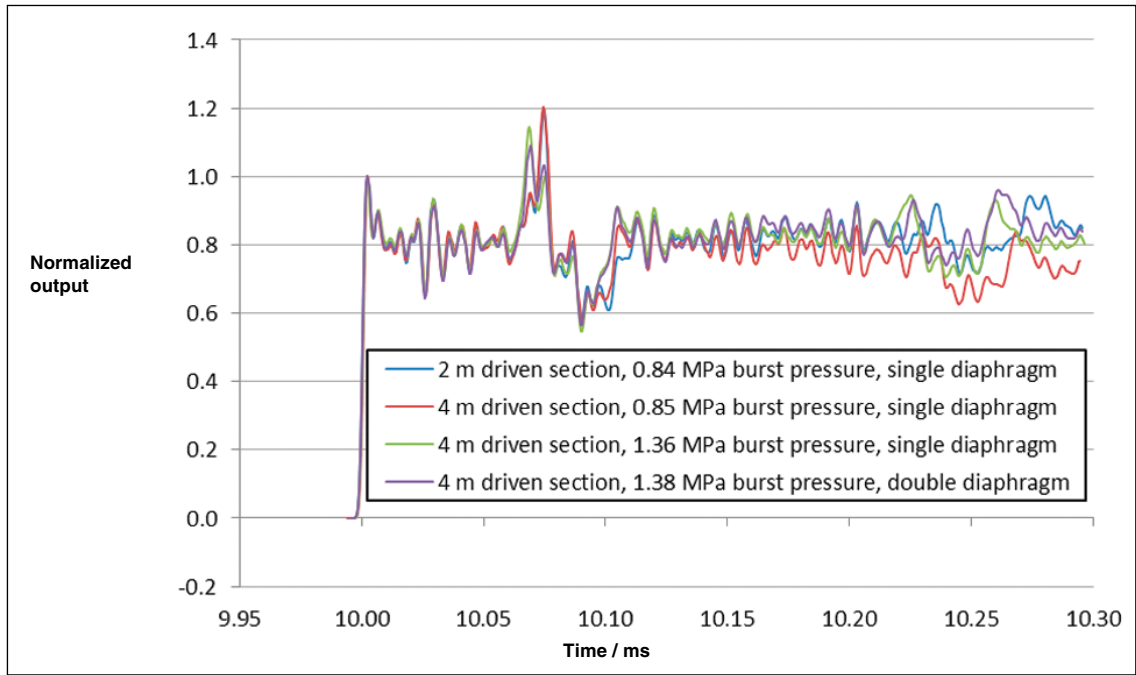


Figure 10: Effects of driven section length, driver section pressure, and diaphragm configuration.

reduced the magnitude of the previously identified characteristic, lending support to the hypothesis that this was the result of pressure variations initiated at the sensor mount/tube interface when the shock front arrived. Any disturbances originating from the area around the tube wall, travelling at the speed of sound in the heated gas behind the reflected shock front (approximately  $490 \text{ m}\cdot\text{s}^{-1}$ ) will reach the centre of the transducer diaphragm after an interval of approximately 0.08 ms which is consistent with the results obtained.

The pre-modification traces also show disturbances to an underlying flat response at about 0.24 ms after arrival of the shock front – this could be explained by the pressure waves generated at

the tube edge ‘bouncing’ across the face of the sensor mount, travelling a distance of three radii before impinging on the transducer’s face for a second time. These effects, although much smaller in magnitude, are still apparent when using the modified mount.

**8.5 Driven pressure values**

The driven section of the tube is able to have its initial pressure varied, to either above or below atmospheric pressure, to vary the amplitude and speed of the pressure step. A set of three tests was performed with the initial driven section absolute air pressure being set to 0.008 MPa, 0.034 MPa,

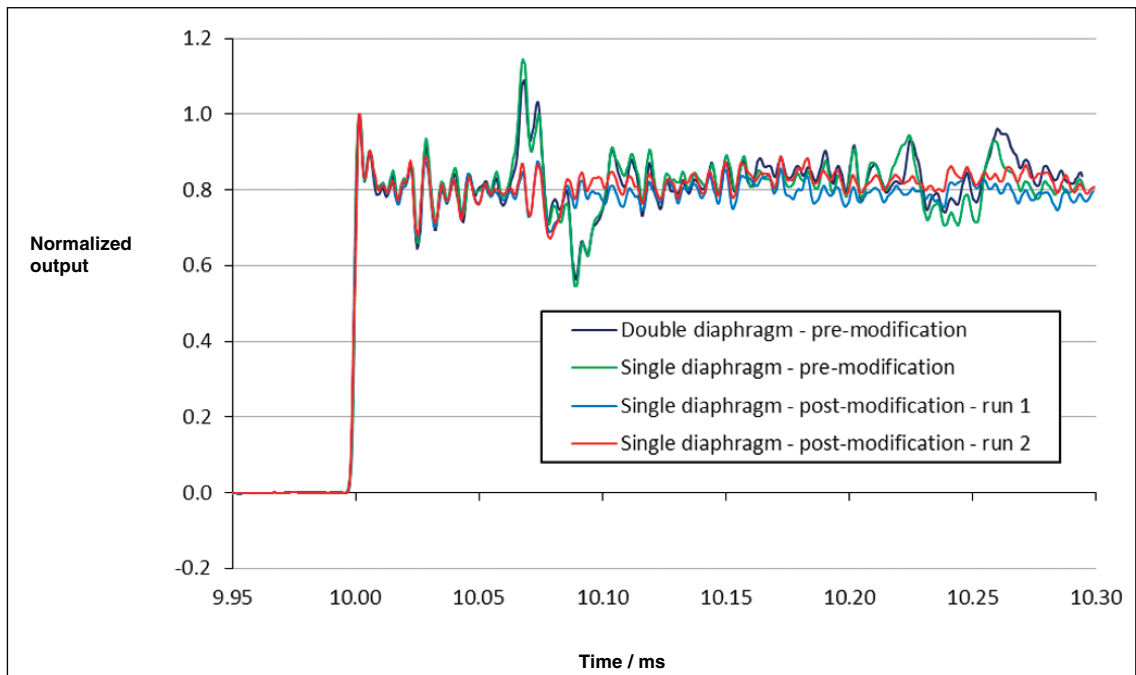


Figure 11: Effect of transducer mount modification.

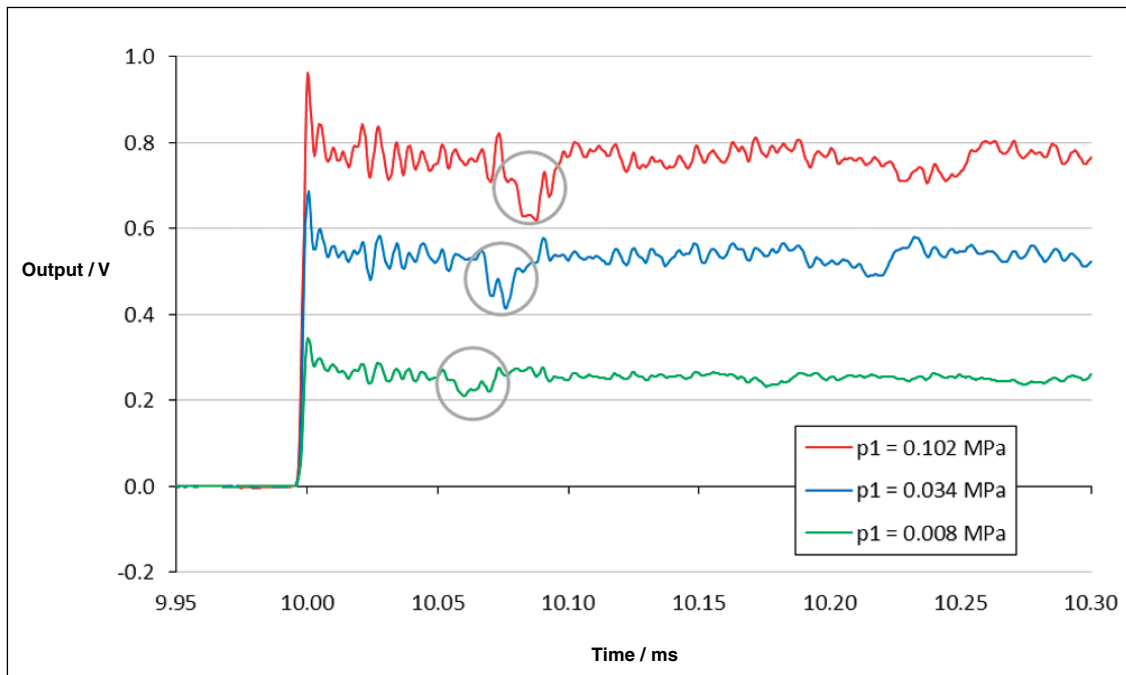


Figure 12: Effect of varying initial driven section pressure.

and 0.102 MPa, using the 0.05 mm brass diaphragm material (figure 12).

The results demonstrate an increase in pressure step magnitude with an increase in initial pressure in the driven section; shock front velocity measurements also agree with theory, showing an increase in velocity with a decrease in driven section pressure (from 554 m·s<sup>-1</sup> at 0.102 MPa, through 680 m·s<sup>-1</sup> at 0.034 MPa, to 864 m·s<sup>-1</sup> at 0.008 MPa). When the normalized output traces are plotted against time (figure 13), the first anomalous portion can be seen to occur at different times (these events are also indicated by the grey circles in figure 12) – this is explained by the increase in speed of sound in the gas caused by the

higher temperatures resulting from the tests with lower pressure in the driven section (figure 4). The second anomalous section also arrives correspondingly earlier in the lower pressure tests (at around 10.17 ms when  $p_1 = 0.008$  MPa and 10.21 ms when  $p_1 = 0.034$  MPa, as opposed to 10.24 ms when  $p_1 = 0.102$  MPa).

### 8.6 Driven gas

As shown in the theory section, the two gas species used within the driver and driven sections affect the magnitude of the generated pressure step. Two pairs of tests were carried out with the 0.1 mm brass diaphragm material using first helium and then argon

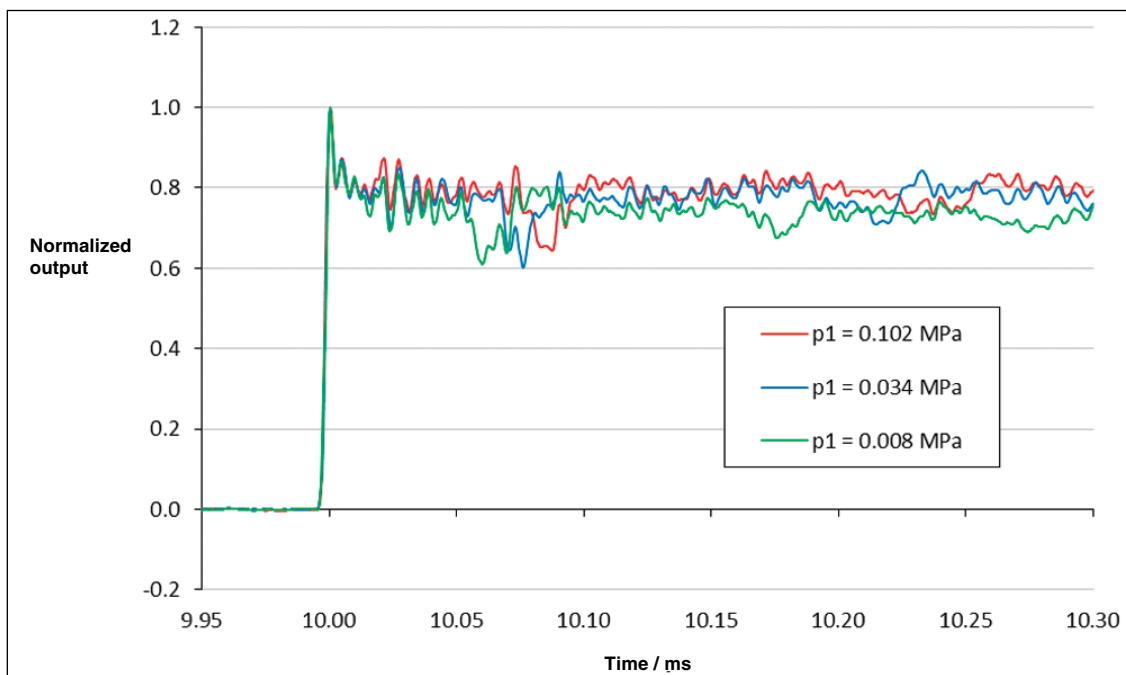


Figure 13: Normalized results showing effect of varying initial driven section pressure.

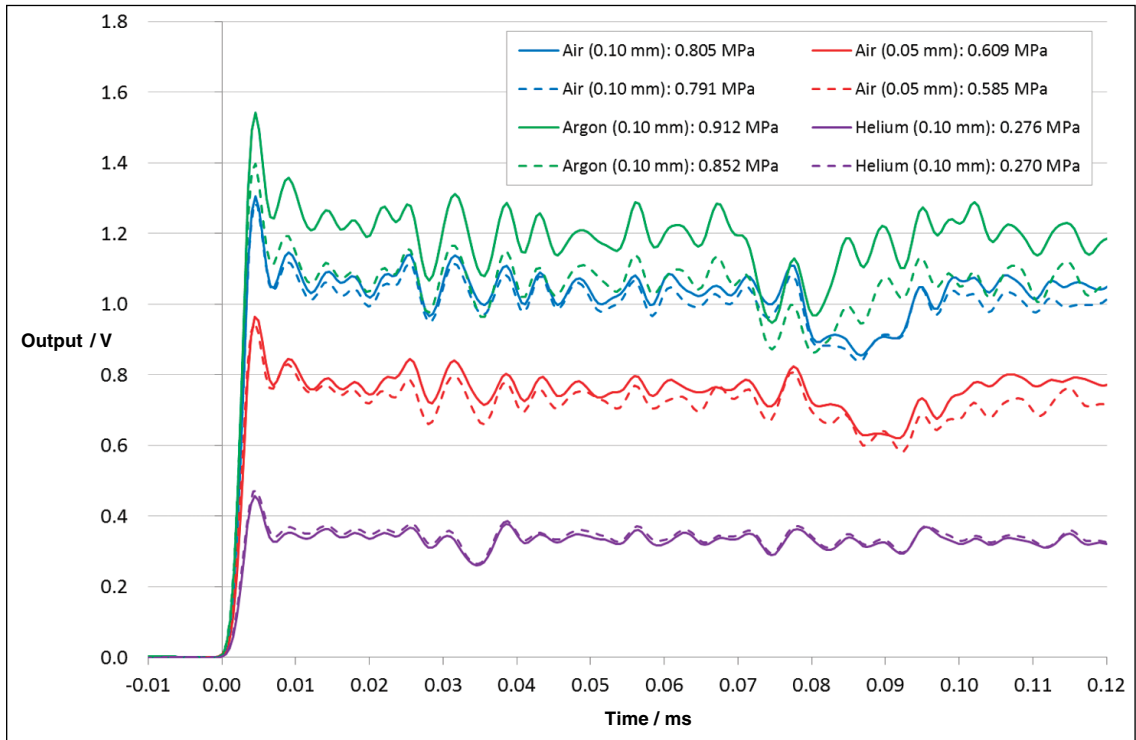


Figure 14: Variation of driven section gas species.

(both nominally at atmospheric pressure) within the driven section, and the resulting measurements compared with the traces obtained with air in the driven section, for both thickness diaphragms. For each trace, given in figure 14, the magnitude of the generated pressure step at the tube end, calculated from the ideal gas theory, is given within the key. The waveforms are plotted in terms of voltage rather than pressure to emphasize that voltage is the quantity recorded and that the static sensitivity of the gauge is not necessarily correct on this timescale.

If we assume that the value of the pressure step calculated from theory is correct and remains constant throughout the period of the measurement, it is possible to calculate the instantaneous sensitivity of the sensor. Figure 15 shows the results replotted as the sensitivity of the sensor in units of  $\text{pC}\cdot\text{bar}^{-1}$ . This simplifies comparison with the sensor's static sensitivity of  $-4.759 \text{ pC}\cdot\text{bar}^{-1}$ , as determined by its manufacturer.

The agreement between the four dynamic traces (which are derived from the means of each pair of

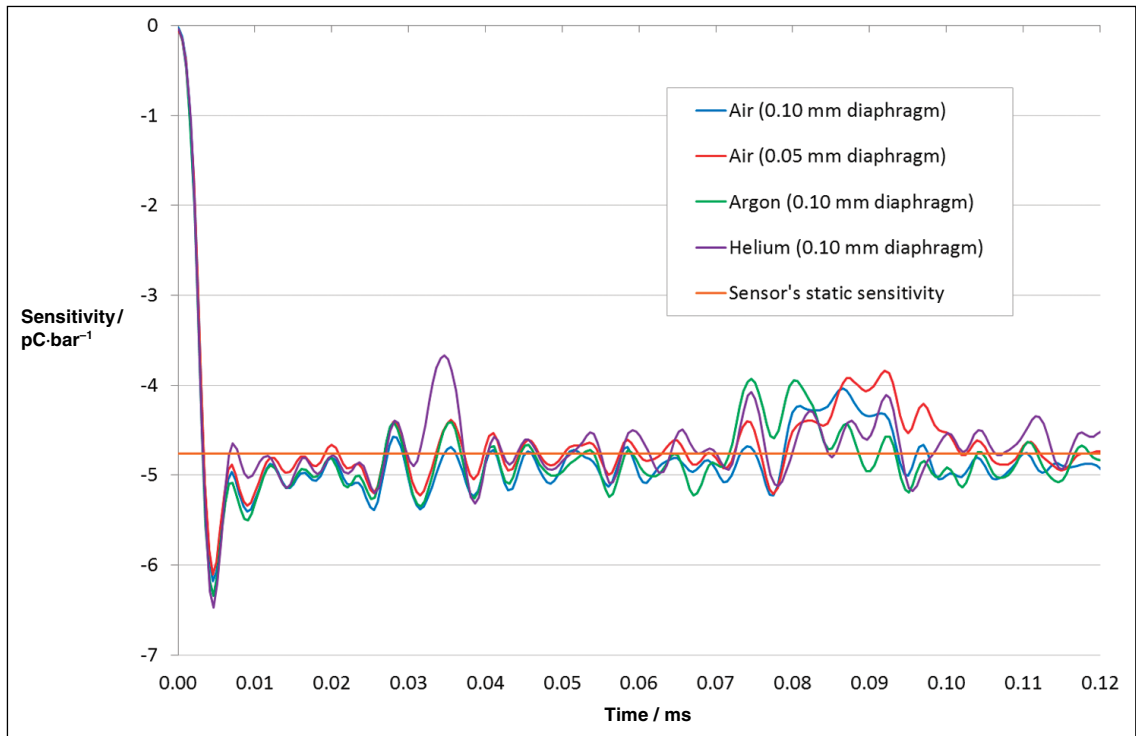


Figure 15: Pressure sensor sensitivity in response to pressure step.

traces given in figure 14), both in terms of absolute magnitude and in terms of amplitude and frequency content around the underlying trend, gives confidence that the theory is correctly predicting the behaviour of the gas within the tube. Discrepancies between the traces, such as the early arrival of the anomalous portion within the helium trace, can be explained by factors such as the much faster speed of sound in the lighter gas. The agreement with the sensor's static sensitivity gives further confidence that the pressure step is being calculated correctly.

Comparison of the results in figure 15 assumes that the sensor has a linear response; in subsequent work the linearity condition can be relaxed by generating pressure steps which are calculated to be identical in different gas species. As long as the sensor response is not affected by gas species, the linearity of the sensor does not affect the result and allows uncertainties due to the operation of the shock tube to be assessed at a number of pressures. The results can then be used to assess the linearity of the sensor.

The possibility that a significant proportion of the dynamic content of the waveforms might be due to the mechanical vibration of parts of the shock tube apparatus, rather than the transducer itself, still needed to be investigated.

### 8.7 Sensor mount block material

Although the sensor is designed to be insensitive to acceleration, the magnitudes of the accelerations generated by the shock wave in the sensor mounting block are very high. In order to determine how much of the frequency content of the transducer

output might be due to acceleration, as opposed to its inherent dynamic response to a pressure step, sensor mounting blocks of different material, but identical geometry, were manufactured to enable accelerations of different amplitude and frequency to be applied to the sensor. Figure 16 gives typical responses from steel, aluminium, and brass mounts.

Although the underlying characteristics obtained from the three mounts are broadly similar, there are significant differences in the amplitudes of the variation about this underlying trend. The increased amplitudes of the dynamic components recorded during the aluminium and brass sensor mount tests, when compared with the steel mount, suggest that vibration of these components may be a significant factor in the sensor output. The elastic modulus of aluminium is approximately three times lower than that of steel, and that of brass a factor of approximately two times lower, suggesting that the resulting dynamic elastic strains within sensor mounts of these materials may be significantly higher than those in a steel sensor mount when subjected to the same step force input.

In order to compare the frequency content of the outputs obtained using the three different block materials, a basic Fourier transform of the time series data was performed, and the results are shown in figure 17.

These plots further demonstrate that the output of the pressure transducer, in response to a step change in input, is strongly influenced by the material of the mount in which it is supported, with frequency peaks (shown circled in grey)

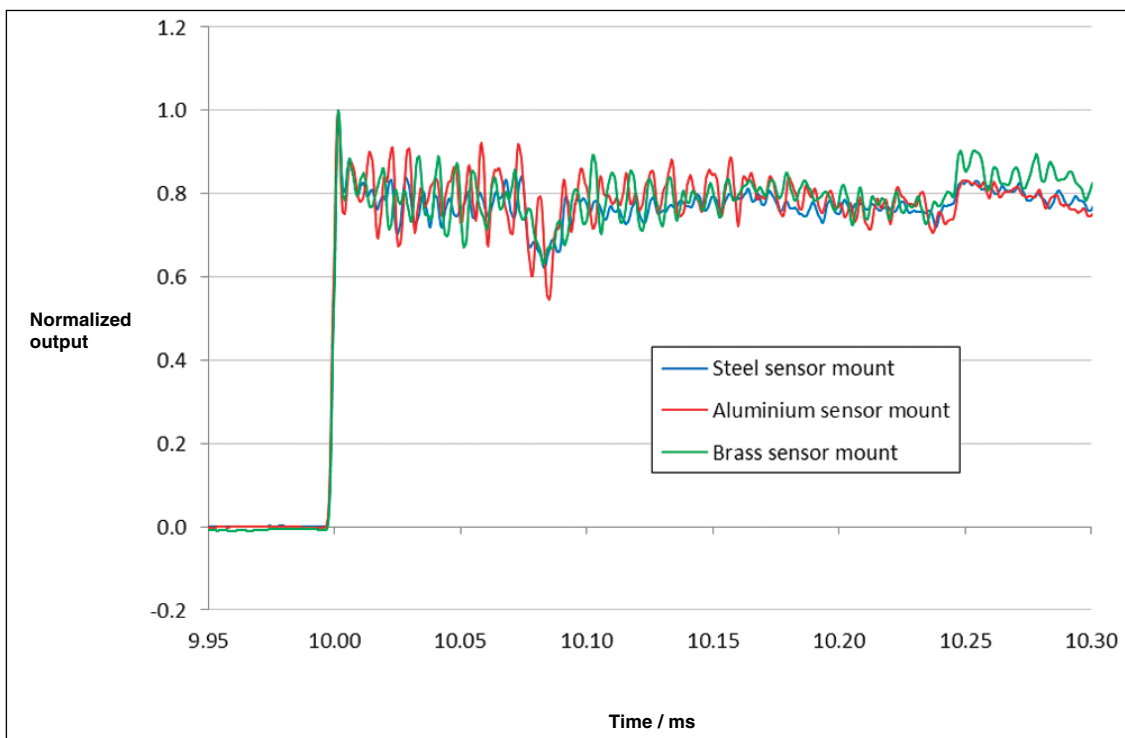


Figure 16: Results obtained with different sensor mount materials.

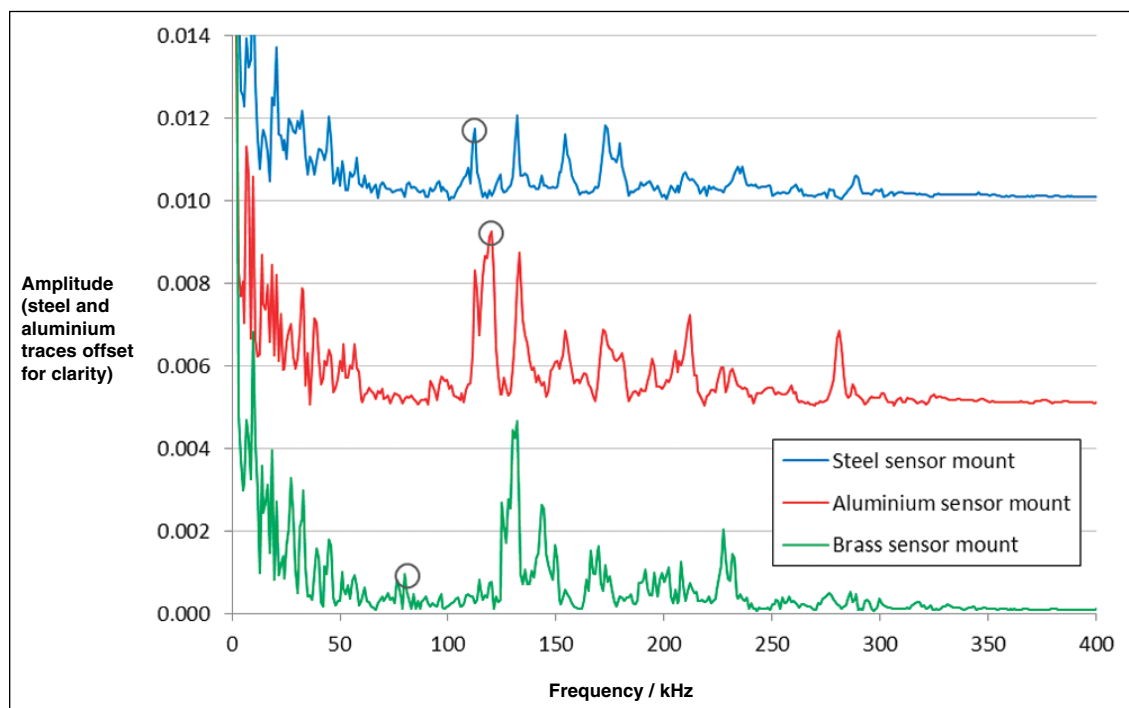


Figure 17: Fourier transform of results obtained with different sensor mount materials.

coinciding with the primary mode of longitudinal vibration for each mount [13] – the lower amplitude of the peak for the brass mount is likely to be due to the sensor’s inbuilt acceleration compensation being more effective at lower frequencies. Vibration of the mount will produce acceleration-induced charges within the sensor, generating spurious signals. Methods to reduce or separate these signals from the underlying pressure response need to be investigated and developed.

## 9 Conclusions

We have developed a novel plastic shock tube and have investigated the effect of diaphragm material, thickness, and configuration, and driven section length, on its operation, and none were found to affect the measured pressure trace significantly. Driven section pressure and gas species were varied and the effects of these variations were found to be consistent with ideal gas theory as applied to a shock tube. The results of the tests performed within the 1.4 MPa shock tube therefore demonstrate that it has the capability to act as a primary dynamic pressure standard, generating extremely rapid pressure steps of calculable magnitude, to characterize the dynamic performance of pressure sensors. As pressure sensors may also be sensitive to acceleration, further work is required to eliminate any effect of acceleration of the sensor mounting block on the calibration result. It should be noted that the method of mounting the sensor in practical applications will be critical to its dynamic performance.

## Acknowledgements

This work is supported by the National Measurement Office, an executive agency of the Department for Business, Innovation & Skills, under its Engineering and Flow Metrology Programme, and has also received support from the European Metrology Research Programme (EMRP). The EMRP is jointly funded by the EMRP participating countries within EURAMET (the European Association of National Metrology Institutes) and the European Union.

## References

- [1] T. J. Esward, *Analysis of Dynamic Measurements: New Challenges Require New Solutions*, XIX IMEKO World Congress, Lisbon, Portugal, 2009.
- [2] S. Eichstädt, *Deconvolution Filters for the Analysis of Dynamic Measurement Process: A Tutorial*, *Metrologia*, 47, pp. 522–533, 2010.
- [3] C. Bartoli, M. F. Beug, T. Bruns, C. Elster, T. Esward, L. Klaus, A. Knott, M. Kobusch, S. Saxholm and C. Schlegel, *Traceable Dynamic Measurement of Mechanical Quantities: Objectives and First Results of this European Project*, *International Journal of Metrology and Quality Engineering*, 3, pp. 127–135, 2012.
- [4] M. Syrimis and D. N. Assanis, *Knocking Cylinder Pressure Data Characteristics in a Spark-Ignition Engine*, *Journal of Engineering for Gas Turbines and Power*, 125 (2), pp. 494–499, 2003.

- [5] C. Hudsona, X. Gaoa and R. Stoneb, *Knock Measurement for Fuel Evaluation in Spark Ignition Engines*, *Fuel*, 80 (3), pp. 395–407, 2001.
- [6] M. Brunt, C. Pond and J. Biundo, *Gasoline Engine Knock Analysis using Cylinder Pressure Data*, International Congress and Exposition, Detroit, USA, 1998.
- [7] H. J. Pain and E. W. E. Rogers, *Shock Waves in Gases*, *Reports on Progress in Physics*, 25 (1), pp. 287–336, 1962.
- [8] D. W. Holder and D. L. Schultz, *On the Flow in a Reflected-Shock Tunnel*, HMSO, London, 1962.
- [9] J. Teichter, *Design of a Shock Tube*, SP Measurement Technology, Borås, Sweden, 2005.
- [10] R. J. McMillan, *Shock Tube Investigation of Pressure and Ion Sensors Used in Pulse Detonation Engine Research*, Air Force Institute of Technology, Dayton, USA, 2004.
- [11] E. L. Petersen and R. K. Hanson, *Nonideal Effects Behind Reflected Shock Waves in a High-Pressure Shock Tube*, *Shock Waves*, 10 (6), pp. 405–420, 2001.
- [12] S. Li, W. Ren, D. F. Davidson and R. K. Hanson, *Boundary Layer Effects Behind Incident and Reflected Shock Waves in a Shock Tube*, 28th International Symposium on Shock Waves, Manchester, United Kingdom, 2012.
- [13] S. Downes, A. Knott and I. Robinson, *Determination of Pressure Transducer Sensitivity to High Frequency Vibration*, IMEKO 22nd TC3, 12th TC5 and 3rd TC22 International Conferences, Cape Town, South Africa, 2014.